Stem Cell Reports
Article

ISSCR

OPEN ACCESS

Advanced Single-Cell Mapping Reveals that in hESC Cardiomyocytes Contraction Kinetics and Action Potential Are Independent of Myosin Isoform

Natalie Weber,[1,6,*] Kathrin Kowalski,[1,6] Tim Holler,[1] Ante Radocaj,[1] Martin Fischer,[2] Stefan Thiemann,[2] Jeanne de la Roche,[2] Kristin Schwanke,[3] Birgit Piep,[1] Neele Peschel,[1] Uwe Krumm,[1] Alexander Lingk,[1] Meike Wendland,[1] Stephan Greten,[1,5] Jan Dieter Schmitto,[3] Issam Ismail,[3] Gregor Warnecke,[3] Urs Zywietz,[4] Boris Chichkov,[4] Joachim Meißner,[1] Axel Haverich,[3] Ulrich Martin,[3] Bernhard Brenner,[1] Robert Zweigerdt,[3] and Theresia Kraft[1]

[1]Institute of Molecular and Cell Physiology, Hannover Medical School, Carl-Neuberg Straße 1, 30625 Hannover, Germany
[2]Institute of Neurophysiology, Hannover Medical School, Carl-Neuberg Straße 1, 30625 Hannover, Germany
[3]Leibniz Research Laboratories for Biotechnology and Artificial Organs (LEBAO), Department of Cardiothoracic, Transplantation and Vascular Surgery, Hannover Medical School, Carl-Neuberg Straße 1, 30625 Hannover, Germany
[4]Laser Zentrum Hannover e.V., Hollerithallee 8, 30419 Hannover, Germany
[5]Present address: Clinic for Neurology, Hannover Medical School, Carl-Neuberg Straße 1, 30625 Hannover, Germany
[6]Co-first author
*Correspondence: weber.natalie@mh-hannover.de
https://doi.org/10.1016/j.stemcr.2020.03.015

SUMMARY

Human pluripotent stem cell-derived cardiomyocytes (hPSC-CMs) represent an attractive model to investigate CM function and disease mechanisms. One characteristic marker of ventricular specificity of human CMs is expression of the ventricular, slow β-myosin heavy chain (MyHC), as opposed to the atrial, fast α-MyHC. The main aim of this study was to investigate at the single-cell level whether contraction kinetics and electrical activity of hESC-CMs are influenced by the relative expression of α-MyHC versus β-MyHC. For effective assignment of functional parameters to the expression of both MyHC isoforms at protein and mRNA levels in the very same hESC-CMs, we developed a single-cell mapping technique. Surprisingly, α- versus β-MyHC was not related to specific contractile or electrophysiological properties of the same cells. The multiparametric cell-by-cell analysis suggests that in hESC-CMs the expression of genes associated with electrical activity, contraction, calcium handling, and MyHCs is independently regulated.

INTRODUCTION

Human pluripotent stem cell-derived cardiomyocytes (hPSC-CMs) present a promising model to investigate human cardiac diseases *in vitro*, as has been shown for hypertrophic, dilated, and other cardiomyopathies (Jung and Bernstein, 2014).

However, it is challenging to overcome the often incomplete and inhomogeneous state of maturation of *in vitro*-derived hPSC-CMs (van Meer et al., 2016; Veerman et al., 2015). Analyses of hPSC-CM populations revealed certain heterogeneity of different contractile protein isoforms and functional properties in the individual CMs (Iorga et al., 2018; Kane and Terracciano, 2017). It was shown that the two cardiac myosin heavy chain (MyHC) isoforms (α-MyHC and β-MyHC), which mainly determine contraction force and shortening velocity of the sarcomeres (Locher et al., 2009), are also quite heterogeneously expressed in individual hPSC-CMs (Weber et al., 2016).

During early stages of cardiac development, human embryonic ventricles display a high expression of α-MyHC (encoded by *MYH6*), while the slow β-MyHC isoform (encoded by *MYH7*) increases from the later embryonic stages on and clearly predominates during fetal development (Racca et al., 2016; Reiser et al., 2001; Wessels et al., 1991). Pioner et al. (2016) showed that the contractile function of long-time cultivated human induced PSC-CM (hiPSC-CM) myofibrils is similar to human fetal myofibrils, both with predominant β-MyHC isoform composition. In the healthy adult human ventricle, β-MyHC accounts for more than 90% of MyHC protein. In human atria both fast α-MyHC and slow β-MyHC are common (Gorza et al., 1984). Yet adult human ventricular and atrial CMs not only express different MyHC isoforms but also show different functional characteristics regarding electrophysiology, calcium handling, and contractility. Human adult atrial CMs in comparison with human adult ventricular CMs show shorter action potential duration (Schram et al., 2002), less extensive T-tubule system with dome-shaped calcium transients (Bootman et al., 2006; Hatem et al., 1997), and faster twitch parameters (Narolska et al., 2005).

For association of hPSC-CM function with isoforms and expression levels of cardiac sarcomeric proteins such as MyHC, often MyHC mRNA expression is used instead of protein analysis. Interestingly, in tissue samples from healthy human ventricles a substantial discrepancy has been observed between the fraction of *MYH6/MYH7*-mRNA and α/β-MyHC protein isoforms (Miyata et al., 2000). Similarly,

analyses at proteome and transcriptome level for many other proteins have shown that mRNA and protein levels are often divergent (Vogel and Marcotte, 2012).

When studying pathomechanisms of familial cardiomyopathies, homogeneous populations of ventricular-like hPSC-CMs are preferable for reliably detecting mutation effects without interference through variable protein isoform expression. We previously showed for human embryonic stem cell-derived cardiomyocytes (hESC-CMs) in comparison with adult cardiomyocytes that different α-MyHC versus β-MyHC protein isoform expression as well as differences in regulatory protein isoforms cause a shift of the force-pCa-relationship, altered tension cost, force generation, and contraction kinetics (Iorga et al., 2018; Weber et al., 2016). With cultivation of hESC-CMs on a stiff matrix such as laminin-coated glass coverslips, a time-dependent switch from mixed expression of α/β-MyHC isoforms toward pure β-MyHC expression at the single-cell level could be induced (Weber et al., 2016). However, even after prolonged cultivation on a stiff surface (up to 70 days) the population of CMs was not homogenously expressing β-MyHC only. The heterogeneity from cell to cell was even larger if CMs were cultivated in floating cardiac bodies (CBs), with >80% of the CMs still expressing variable fractions of both α-MyHC and β-MyHC (Weber et al., 2016).

Since MyHC isoforms have been shown to affect the function of adult CMs, the main aim of this study was to investigate at the single-cell level to which extent twitch contraction kinetics and action potentials (APs) of hPSC-CMs are influenced by the relative expression of α-MyHC versus β-MyHC. To study the effects of various ratios of the two MyHC isoforms on the function of hESC-CMs, we applied two cultivation strategies (plated CMs versus CMs from CBs), which have been shown to promote MyHC isoform expression in single hPSC-CMs differently. Since β-MyHC is a characteristic marker of ventricular specificity, we furthermore asked whether MyHC protein isoform levels or *MYH6*- and *MYH7*-mRNA expression are sufficient to predict ventricular-like versus atrial-like functional hPSC-CM phenotypes.

To address these questions, we developed a partially automated two-dimensional single-cell mapping technique that could be applied independently on different microscopes including setups for contraction analysis and electrophysiology. This methodology enabled us to relocate the individual hPSC-CMs for multiparametric cell-by-cell analysis.

RESULTS

Single-Cell Mapping: Multiparametric Cell-by-Cell Analysis with High Efficiency and Accuracy

Multiple parameters of hESC-CM function as well as protein expression, mRNA expression, and CM morphology were analyzed in hESC-CMs cultivated for 35 days after differentiation on laminin-coated glass coverslips (d15 + 35; plated hESC-CMs), in hESC-CMs cultivated for the same time (d50) as CBs in suspension culture and plated onto coverslips shortly before analysis (CMs from CBs) (Figure 1A).

To characterize multiple parameters for the very same CM, it was essential to establish a method that allows to combine data derived from different setups including standard microscopes and non-standard systems for measurements of contraction and electrophysiology of hESC-CMs (Figures 1B–1D). This required retrieval of the individual CMs at different microscopes after accurate two-dimensional cell mapping. In addition, for combining analyses of contraction and electrophysiology with morphological and expression parameters on the same single cells, the coverslips with the cells had to undergo different experimental procedures between the measurements. For this, the coverslips had to be removed from the setup where the original coordinates were recorded. When the coverslips were transferred back to another or even the same microscope, the coverslip and, thus, the CMs were not positioned automatically at the same coordinates. To overcome this, in our method we implemented a feature to directly correct for changes in position.

Our approach (Figures 1B–1D) is based on digital x-y calipers on each microscope to precisely mark and relocate fixed reference points and the position of the CMs on each coverslip. Automatic recalculation of the coordinates allows correction for shifts and rotations in positions of the coverslip, enabling efficient cell remapping.

Due to the precision of the calipers and the unbiased recording of the coordinates, every remapped CM was visible at 40× magnification in the very center of the field of view of the respective microscope used in the subsequent analysis. Thereby, unequivocal identification of each cell is warranted without searching efforts. Since plated hESC-CMs typically have characteristic morphologies, their identification was additionally confirmed by images taken at 10× and 40× magnification after functional measurements.

The method's accuracy allowed retrieval of 97% of all mapped cells after the transfer from fluorescence *in situ* hybridization (FISH)-based mRNA analysis to immunostaining and protein analysis at another microscope (Figures 1C and 1D). After sample transfer from twitch recording to protein analysis, 84% of all mapped cells were retrieved (Figures 1B and 1D); processing-induced cell loss impeded an even higher recovery rate. Remapping was less efficient after patch-clamp experiments, since retraction of the patch pipette occasionally damaged the cell membrane, promoting the likelihood of subsequent cell loss. Nevertheless, 44% of all patched cells were still recovered, whereby

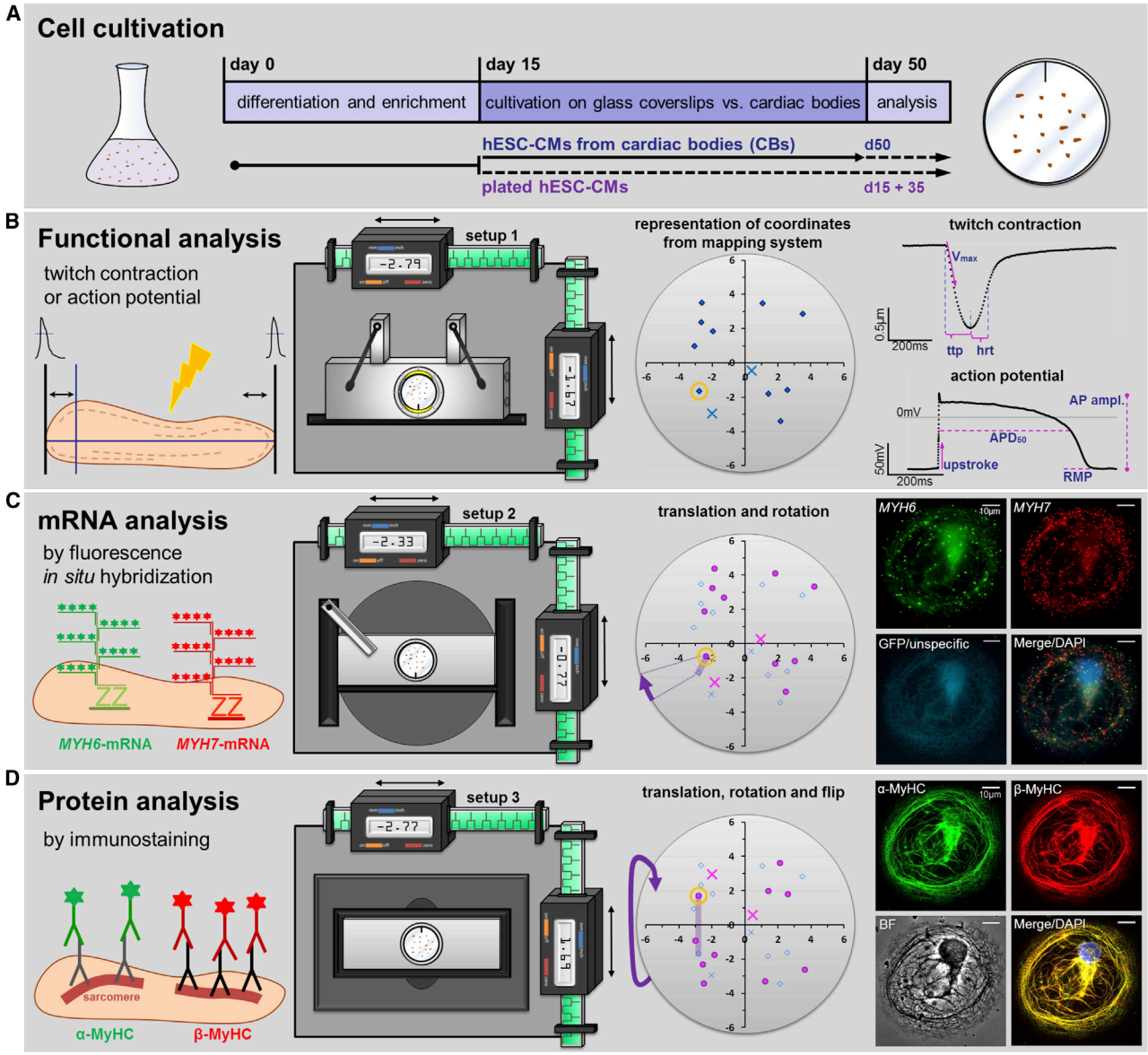

Figure 1. hESC-CM Cultivation and Cell-Mapping Technique

(A) Differentiation, enrichment, and cultivation strategy for hESC-CMs. Continuous line, cultivation of hESC-CMs in CBs; dashed line, cultivation of CMs plated on coverslips.

(B) From left to right: schematic representation of measurement of electrically stimulated contraction or action potential (AP) of a single CM in experimental "setup 1", of coordinates of mapped CMs in field of view (blue diamonds), and of sample recordings of twitch contraction or action potential. Reference points for cell-mapping technique (light-blue crosses) and the example cell (orange circle) mapped at the coordinates shown in the displays of the calipers of "setup 1." This cell is retrieved in the subsequent analysis steps.

(C) Scheme of FISH labeling of *MYH6* and *MYH7*-mRNAs, of "setup 2" for FISH analysis, and of new coordinates of cells due to translation and rotation of the coverslip (purple arrow) upon mounting on another microscope. New positions of the CMs (magenta circles), old positions of CMs in the background (blue diamonds), and the actual positions of the two reference points (magenta crosses). Right: four images showing sample cell in three fluorescence channels with both *MYH*-mRNAs (green, red), unspecific fluorescence (cyan), and merged image.

(D) Scheme of immunofluorescent staining with α-MyHC- and β-MyHC-specific antibodies for protein categorization of the CMs. Note that the coverslip was flipped upside down to accommodate the different optical settings (purple arrow). Actual positions of the CMs after staining are shown as magenta circles. The images on the right show the same CM as in (C) co-expressing both α-MyHC (green) and β-MyHC (red) isoforms, as well as a bright-field image and a merged image.

See also Supplemental Experimental Procedures.

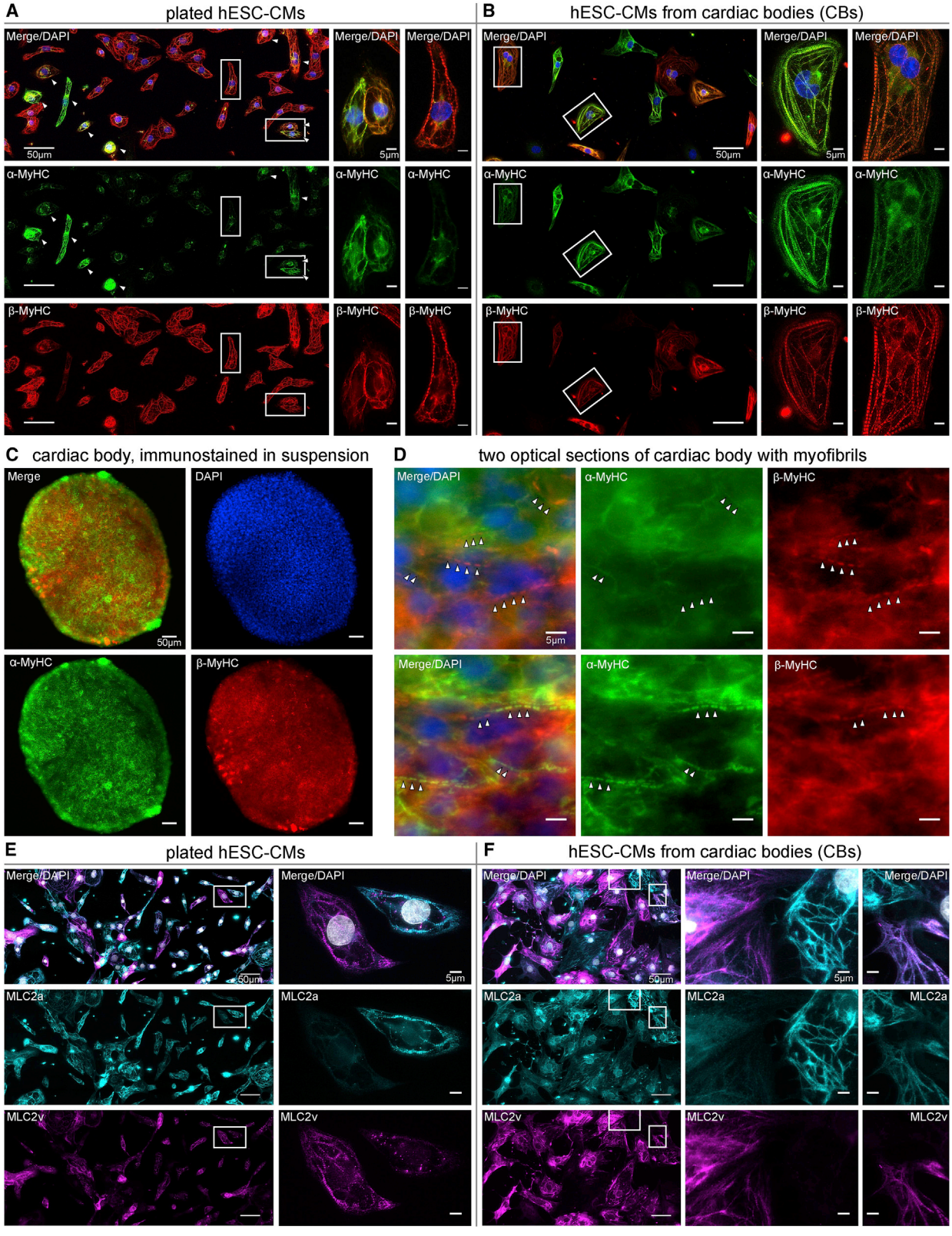

(legend on next page)

plated CMs appeared more stable (49% retrieved CMs) and CMs from CBs were more prone to detachment (39% retrieved CMs).

Heterogeneous Expression of MyHC and Myosin Light Chain Protein Isoforms in hESC-CMs

To analyze the co-expression of MyHC or myosin light chain (MLC) isoforms at the single-cell level, we visualized the protein expression of the ventricular versus atrial markers β-MyHC and myosin regulatory light chain 2 (MLC2v versus MLC2a). Expression was analyzed not only in plated hESC-CMs (d15 + 35) and in CMs from CBs (d50), but for MyHC also at the level of undissociated CBs and their myofibrils (d50). Figure 2A shows an overview of plated CMs stained for α-MyHC (green) and β-MyHC (red), with about three-quarters of the CMs expressing pure β-MyHC and no detectable α-MyHC in the sarcomeres. Interestingly, for CMs from CBs the fraction of CMs with pure β-MyHC expression was much smaller (Figure 2B). In both cases CMs showed heterogeneous co-expression of both cardiac MyHC isoforms, ranging from pure β-MyHC expression to CMs with different proportions of both MyHC isoforms and pure α-MyHC expression. Notably, staining of hESC-CMs at the level of whole CBs *in situ* (Figures 2C and 2D) confirmed the level of heterogeneity of MyHC isoform expression in CMs from CBs on coverslips.

These observations are in contrast to adult, human ventricular myocardium, where the majority of the CMs show pure β-MyHC expression at the single-cell level. Only occasionally are single CMs with mixed expression of both cardiac MyHC isoforms found (Figure S1A). In human adult atrial tissue, essentially all CMs show α-MyHC expression but with variable fractions of β-MyHC in some CMs (Figure S1B).

Another marker of ventricular CMs is MLC2v (Morano, 1999). We stained plated hESC-CMs and those from CBs for MLC2v and MLC2a. For both types of CMs heterogeneous expression of both MLC2 isoforms was observed (Figures 2E and 2F). This is different from adult human ventricular tissue, which essentially lacks MLC2a expression (Figure S2A). In adult human atrial tissue MLC2a is the dominant isoform, although occasionally cells with predominant MLC2v expression were observed (Figure S2B).

The heterogeneous populations of hESC-CMs are ideally suited to characterization of specific functional parameters (e.g., twitch and AP) in direct relation to sarcomeric protein isoform and mRNA expression of individual CMs. Here, we focused on the effects of α-MyHC versus β-MyHC isoform expression on CM contraction and electrical activity.

Quantification of α/β-MyHC Protein and *MYH6*/*MYH7*-mRNA Isoform Expression in Individual hESC-CMs

To relate ventricular-like versus atrial-like hESC-CM function to the relative expression levels of MyHC isoforms in individual CMs, we established quantification of the relative abundance of the two isoforms at protein and mRNA levels. For MyHC protein analysis, fixed CMs were categorized with respect to sarcomeric signal intensity of α-MyHC and β-MyHC immunostaining (Figure 3A; see details for scoring and categorization criteria of MyHC and MLC staining in Figures S3A and S3B). Figure 3B shows the fractions of the five categories for individual plated CMs and CMs from CBs in different hESC-CM batches. On average, 75% of plated CMs expressed pure β-MyHC and only 2% expressed pure α-MyHC. However, 23% of the plated cells still showed heterogeneous co-expression of both α-MyHC and β-MyHC isoforms. An even larger fraction of on average 68% of CB-derived cells co-expressed both MyHC isoforms, while 23% had pure α-MyHC and only 9% pure β-MyHC. Interestingly, co-immunostaining revealed that these functionally quite different MyHC isoforms were often co-identified in the same sarcomeres (Figure 3A).

In contrast to MyHC isoform expression, on average 49% of all plated hESC-CMs had pure MLC2a (Figure S3C). Although about 75% of these CMs were expressing pure β-MyHC (Figure 3B), only few expressed pure MLC2v (9%, Figure S3C), suggesting independent regulation of expression of these proteins in the hESC-CM model. The majority of CMs from CBs co-expressed the two MLC2 isoforms. Somewhat unexpectedly, 54% of the CMs from CBs showed pure or predominant MLC2v isoform expression, in contrast to only 18% of the plated CMs (Figure S3C). Taken together, the data suggest that in plated CMs as well as in CMs from CBs, ventricular isoforms of MyHC and MLC2 are rarely co-expressed. Cultivation on a stiff

Figure 2. Heterogeneous Expression of MyHC and MLC2 Isoforms in hESC-CMs

(A–D) Immunostaining of (A) plated hESC-CMs, (B) CMs from CBs, and (C) whole CB against β-MyHC (red) and α-MyHC (green). Scale bars, 50 μm. Insets show single CMs (A and B; scale bars, 5 μm). (D) Myofibrils in CBs (arrows) with different MyHC compositions. Scale bars, 5 μm.

(E and F) Plated hESC-CMs (E) and CMs from CBs (F) immunostained against MLC2v (magenta) and MLC2a (cyan). Scale bars, 50 μm. Insets show single CMs with different MLC2 compositions. Scale bars, 5 μm. DAPI (blue) staining of nuclei.

See also Figures S1, S2, and S3.

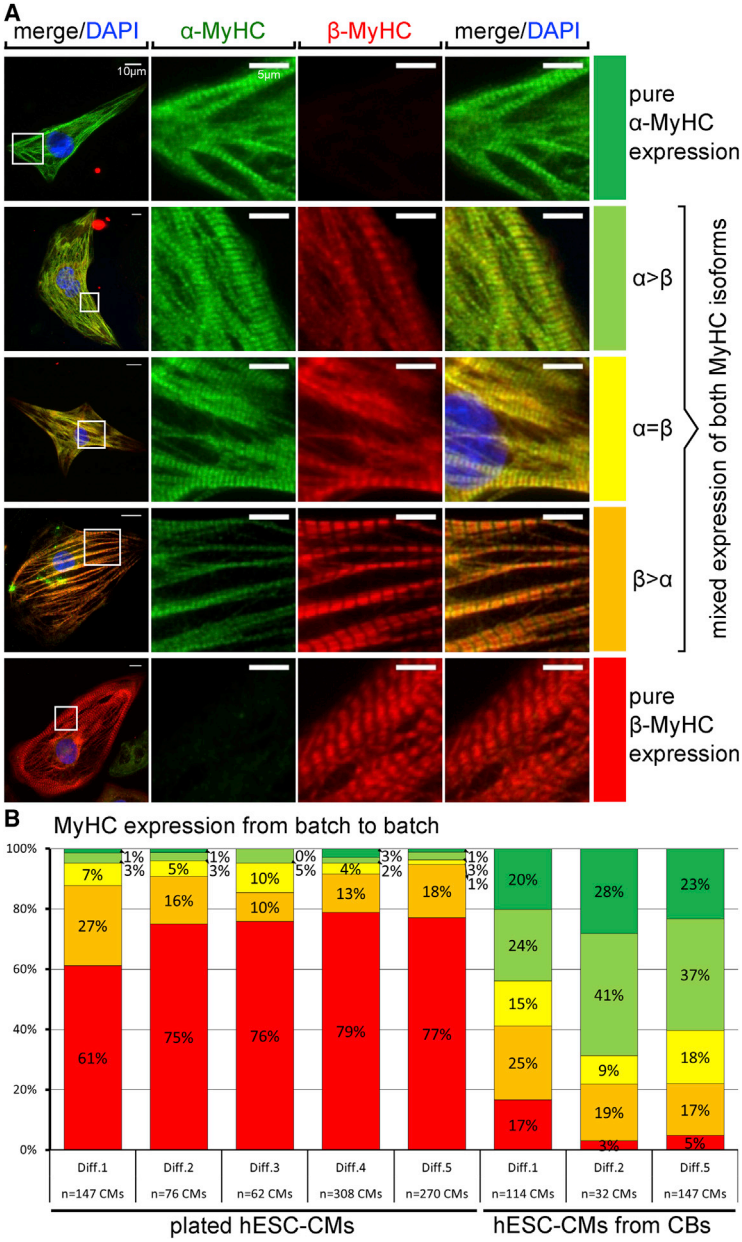

Figure 3. Heterogeneous α-MyHC versus β-MyHC Protein Expression from Cell to Cell

(A) Sample hESC-CMs representing the different categories from pure α-MyHC- to pure β-MyHC-positive CMs with three categories of CMs with mixed α/β-MyHC expression (top to bottom). Left column: merged images of single CMs with marked regions of interest. Scale bars, 10 µm. Middle columns: zoomed regions of sarcomere striation pattern with fluorescent labeling specific for α-MyHC (green) and β-MyHC (red). Scale bars, 5 µm. Right column: merged images (blue, DAPI). Scale bars, 5 µm. Color code indicates protein fluorescence category (α, α > β, α = β, β > α, β) of each displayed CM.

(B) Fractions of total number (n) of individual CMs in the different categories of MyHC protein isoform expression as revealed by fluorescent labeling for plated hESC-CMs and hESC-CMs from CBs. Each column represents an independently differentiated batch (Diff.) of hESC-CMs. Each CM was categorized as shown above and explained in Figure S3.

matrix seems not to favor the ventricular MLC2 isoform, in contrast to the β-MyHC isoform expression.

For quantification of the relative expression of the two MyHC isoforms at mRNA level, FISH was used. The specificity of both *MYH*-mRNA probe sets was tested with human adult ventricular and atrial tissues as shown in Figure S4. Analysis of *MYH6*- versus *MYH7*-mRNA revealed variable fractions of the two *MYH*-mRNAs and variable total counts of the respective mRNA spots from cell to cell (Figure 4). For plated CMs, on average 84% *MYH7*-mRNA spots and 16% *MYH6*-mRNA spots were detected. For individual CMs, however, the fraction of *MYH7*-mRNA ranged from 3% to 100% (Figure 4A). The absolute numbers of mRNA spots for the same cells as in Figure 4A indicated a highly variable mRNA content for individual CMs, with spot counts up to 1,223 for *MYH6*-mRNA (green bars) and up to 2,753 for *MYH7*-mRNA (red bars; Figure 4B).

For CMs from CBs an even larger cell-to-cell variability of *MYH6*- versus *MYH7*-mRNA fractions was observed (Figure 4C). On average 39% *MYH6*-mRNA spots and 61% *MYH7*-mRNA spots were counted, while the range for individual CMs was from 2% to 98% for both mRNAs. Not only

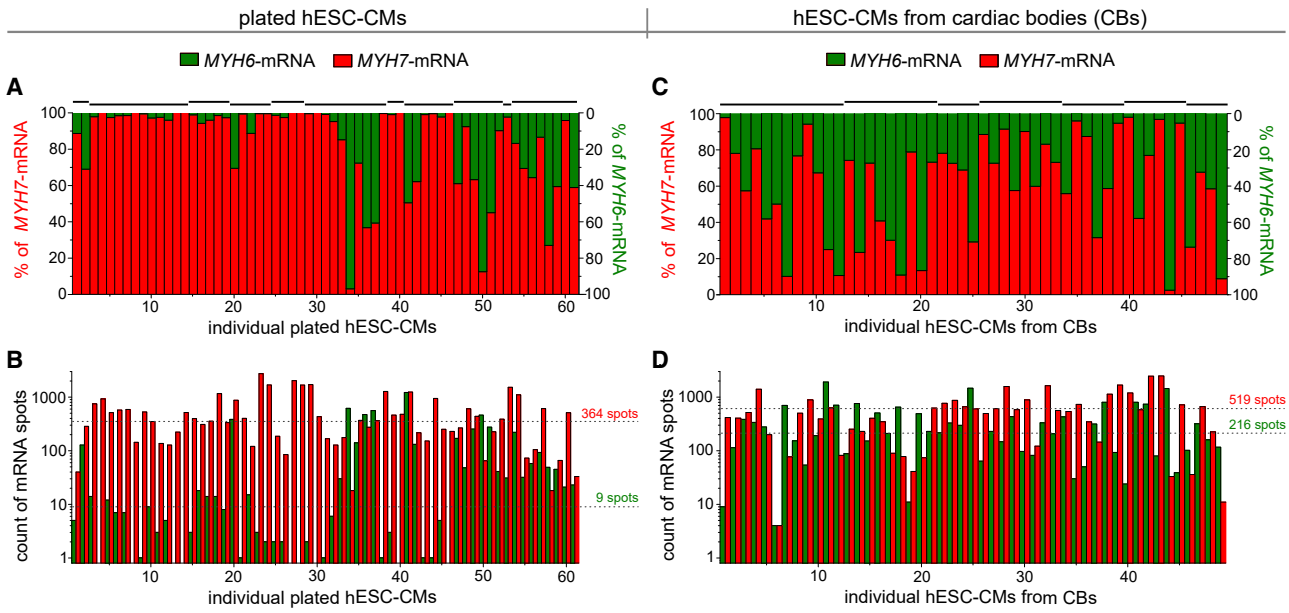

Figure 4. FISH Analysis of *MYH6*-mRNA versus *MYH7*-mRNA Expression Reveals Highly Variable Fractions and Absolute Counts of Both *MYH*-mRNAs from Cell to Cell

Fractions of (A) *MYH6*-mRNA (green) and (C) *MYH7*-mRNA (red) in individual plated hESC-CMs (A) and hESC-CMs from CBs (C). Black-line segments on top of the bar chart indicate individual coverslips on which the cells were analyzed. Absolute counts of *MYH6*-mRNA spots (green) and *MYH7*-mRNA spots (red) for the same individual plated hESC-CMs (B) as in (A) and for the same hESC-CMs from CBs (D) as in (C). Dashed lines indicate median values for absolute counts of *MYH6* (green) and *MYH7* (red). For plated hESC-CMs, n = 61; for hESC-CMs from CBs, n = 49. See also Figure S4.

the fractions but again also the absolute counts of mRNA spots of both MyHC-mRNAs varied considerably from cell to cell, reaching spot counts of up to 1,923 for *MYH6*-mRNA and up to 2,499 for *MYH7*-mRNA (Figure 4D).

To address the question of whether *MYH*-mRNA levels represent MyHC protein levels in individual CMs and thus could be sufficient to predict ventricular-like versus atrial-like functional hESC-CM phenotypes, we studied the relation between *MYH6/MYH7* mRNA and α/β-MyHC protein expression in the very same CMs. The single-cell mapping technique was used to assign mRNA data from FISH analysis and protein immunostaining data (Figure 5). We observed pronounced heterogeneity of *MYH*-mRNA expression among hESC-CMs as highlighted by examples in Figure 5, including CMs showing only *MYH7*-mRNA and pure β-MyHC protein (Figure 5A), comparable levels of both *MYH*-mRNAs and pure β-MyHC (Figure 5B), and expression of both *MYH*-mRNAs and mixed α/β-MyHC isoforms at the protein level (Figure 5C). Figures 5D and 5E show the fraction of *MYH7*-mRNA of total *MYH*-mRNA in relation to categories of α/β-MyHC protein isoform expression for individual cells. Cultivating CMs on coverslips (Figure 5D) not only induced much higher expression of β-MyHC as compared with CB-derived cells (Figure 5E) but also clearly increased the fraction of *MYH7* versus *MYH6*-mRNA. However, the large scatter of *MYH7*-mRNA fractions for each of the five α/β-MyHC protein categories indicates that there is no clearly predictable relationship between mRNA and protein abundance at the single-cell level.

hESC-CM Contraction Parameters Are Independent of α/β-MyHC Protein Isoform but Change with Cell-Culture Conditions

To test how MyHC isoform composition affects contraction parameters, after functional characterization we immunofluorescently stained CMs for MyHC isoforms. Figure 6A shows representative examples of twitch kinetics of CMs that were electrically stimulated. For the contraction phase, we detected a significantly shorter time to peak (ttp, Figures 6A and 6B) and faster maximum shortening velocity (V_{max}) for plated CMs versus CMs from CBs (Figure 6C). For the relaxation phase, half-relaxation time (hrt) decreased significantly for the plated CMs versus CMs from CBs (Figure 6D).

Since considerable numbers of CMs from CBs as well as plated CMs show heterogeneous MyHC isoform expression (Figure 3B), single-cell mapping was used for consecutive analysis of twitch and MyHC isoform expression of the same CMs. Overall, the values for ttp, V_{max}, and hrt were essentially independent of the α-MyHC and β-MyHC

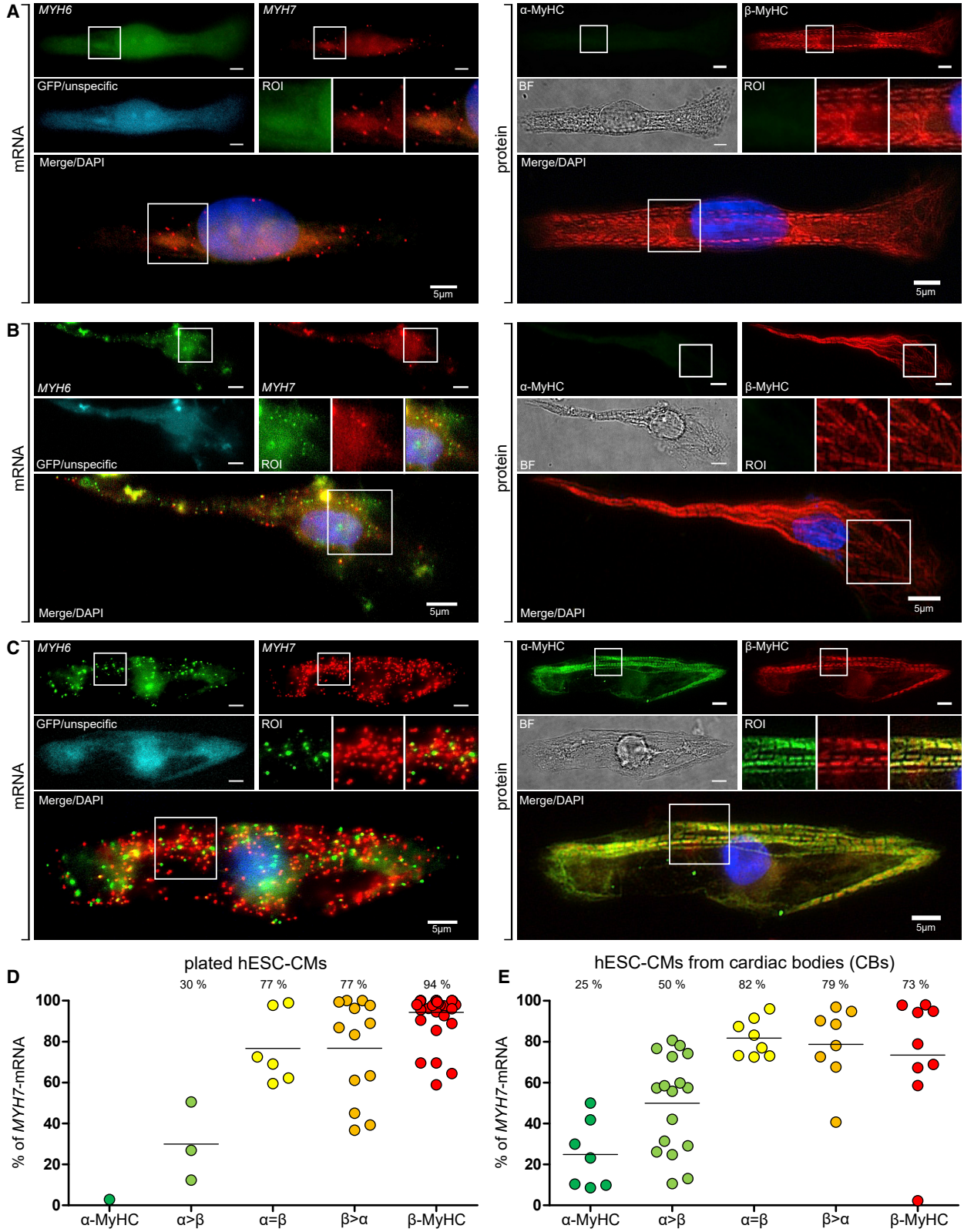

(legend on next page)

isoform composition of individual plated CMs (Figures 6E–6G) and CMs from CBs (Figures 6H–6J), respectively. For plated cells, data indicate that a small fraction of α-MyHC in the sarcomeres (see category β > α) does not affect twitch parameters. For CMs from CBs, which include several predominantly α-MyHC-expressing CMs, also no obvious correlation of MyHC isoform expression and twitch kinetics was observed. Moreover, there was no evidence for a relationship between MyHC isoform and specific time courses of calcium transients or diastolic calcium levels of the hESC-CMs. Figure S5 shows that time courses of intracellular calcium transients and diastolic calcium levels of individual plated CMs and CMs from CBs, as described previously in Weber et al. (2016), are highly heterogeneous, without evidence for distinct populations of transients that would correspond to the different groups of MyHC expression (pure α, α > β, α = β, β > α, pure β).

Systematic differences in resting sarcomere length (SL) and morphology could mask possible effects of the expressed MyHC isoforms on twitch kinetics. Analysis of mean resting SL of plated CMs and for CMs from CB after immunostaining revealed no significant difference (Figure S6A). Also for individual pure α-MyHC versus pure β-MyHC CMs, SL distribution was not systematically different (Figure S6B). We also analyzed cell length and width and aspect ratio (cell length/width) of individual CMs from both CM populations. Overall, CMs from CBs showed significantly larger cell area in comparison with plated CMs, due to both larger length and width of the cells (Figures S6C–S6E). Plated CMs were more elongated in comparison with CMs from CBs, as indicated by a significantly larger aspect ratio (Figure S6F). Under both cultivation conditions the morphological phenotypes and alignment of myofibrils were quite heterogeneous, although in plated CMs myofibrils appeared somewhat more longitudinally oriented.

We also studied twitch kinetics as a function of resting SL and MyHC isoform expression (Figures S6G and S6H). For a given CM, longer SL led to longer ttp and longer hrt of twitch (Figures S6G and S6H, left panels). However, the correlations were weak (R^2 = 0.05–0.29). The contraction amplitude was not altered (data not shown), indicating that shortening velocity decreases with increasing SL. Note that the resting sarcomere lengths were measured after fixation of the CMs. Increased elongation of CMs (larger aspect ratio, Figures S6I and S6J) was weakly associated with shorter ttp and hrt. There was no evidence for a significant effect of MyHC isoform expression on any of these relationships in both plated CMs and CMs from CBs (Figures S6G–S6J, middle and right panels).

Together, the data indicate that the observed differences in ttp, V_{max}, and hrt between plated CMs and CMs from CBs as shown in Figure 6 are not related to morphological parameters but most likely result from other differences induced by the different cultivation strategies, in accordance with previous observations (Lundy et al., 2013; Weber et al., 2016).

Action Potential Properties Are Independent of α/β-MyHC Isoform Expression in hESC-CMs

Based on the distinct electrophysiological properties and MyHC protein expression of atrial versus ventricular adult human CMs, it appears likely that ventricular APs are associated with the β-MyHC isoform, and α-MyHC or mixed MyHC isoform expression is associated with atrial-like APs in individual cells.

To address this question, we conducted patch-clamp experiments in the whole-cell current-clamp mode. Representative recordings from spontaneously active CMs displayed resting membrane potentials (RMPs) of around −65 mV and APs of variable shape and size for plated CMs and CMs from CBs (Figures 7A [upper traces] and 7B). Since AP shape strongly depends on ion-channel properties at resting conditions, we applied negative holding currents (up to 100 pA) to hyperpolarize the cell membrane to more physiological resting potentials around −80 mV and then evoked APs by short depolarizing current injections (0.3–4.8 nA, 1 ms; Figure 7A, lower traces). Continuous hyperpolarization by exogenous current application does not reflect the physiological state of a

Figure 5. No Strict Relationship between *MYH6/MYH7*-mRNA and α/β-MyHC Protein Expression per Individual hESC-CM

Examples of retrieved hESC-CMs with different *MYH*-mRNA (left; *MYH6*-mRNA, green; *MYH7*-mRNA, red; the same single focal plane for both *MYH*-mRNAs is shown) and MyHC protein isoform expression (right; α-MyHC, green; β-MyHC, red).

(A) Left: single CM with exclusively *MYH7*-mRNA spots; no *MYH6*-mRNA specific spots were detected. This hESC-CM showed specific sarcomere staining for β-MyHC isoform only (right). Scale bars, 5 μm; see also zoomed region of interest.

(B) Left: CM with both *MYH6*-mRNA and *MYH7*-mRNA spots, but specific sarcomere staining for β-MyHC isoform only (right). Scale bars, 5 μm.

(C) Left: CM with both *MYH6*-mRNA and *MYH7*-mRNA spots and co-expression of both MyHC isoforms (right). Scale bars, 5 μm.

(D and E) Fraction of *MYH7*-mRNA for hESC-CMs with different MyHC protein expression (ranging from pure α-MyHC- to pure β-MyHC-positive CMs with three categories of CMs with mixed α/β-MyHC expression, α > β, α = β, β > α) for plated hESC-CMs (n = 61; D), and hESC-CMs from CBs (n = 49; E). Horizontal lines and numbers above columns indicate mean values.

See also Figure S4.

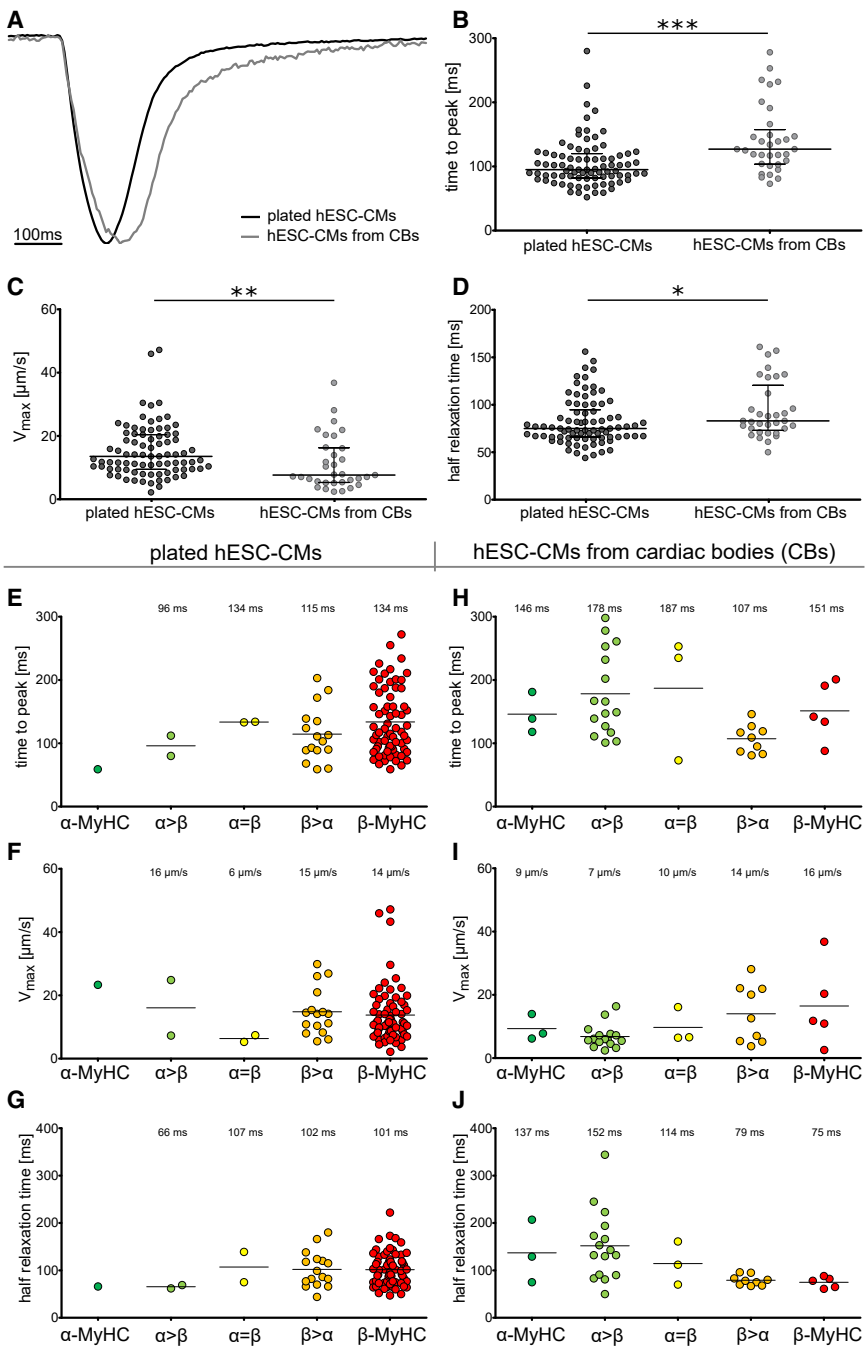

Figure 6. Parameters of Twitch Contraction Are Independent of α/β-MyHC Isoform Expression in Individual hESC-CMs

(A) Normalized averaged traces of original recordings for twitch contraction of plated CMs (black) and CMs from CBs (gray).

(B–D) Time to peak (ttp) of twitch (B), maximum contraction velocity of twitch (V_{max}) (C), and half-relaxation time (hrt) of twitch (D) for plated CMs (dark-gray circles) and CMs from CBs (light-gray circles).

(E–J) ttp of twitch (E and H), V_{max} of twitch (F and I), and hrt of twitch (G and J) of the individual retrieved CMs in the different categories of pure α-MyHC- and pure β-MyHC-positive CMs, with three categories of CMs with mixed α/β-MyHC expression (α > β, α = β, α < β) of plated CMs (n = 90; left column) and CMs from CBs (n = 36; right column).

Horizontal lines in (B) to (D), median ± interquartile range (IQR); in (E) to (J), mean values are indicated (horizontal lines and numbers above columns). Statistical significance was tested by Mann-Whitney U tests with *p < 0.05, **p < 0.01, and ***p < 0.001. See also Figures S3 and S6.

CM. However, artificial hyperpolarization to a common membrane potential is a useful tool for investigating AP parameters under comparable conditions, even though varying expression of K_{ir} channels in hESC-CMs might cause more or less depolarized resting potentials. APs with long plateau phase (>200 ms) appeared ventricular-like, whereas those with shorter APs (20–200 ms) and more triangular shape were classified atrial-like. Some cells generated very short, spike-like APs (<20 ms). Figure 7C shows AP durations at 50% repolarization level (APD_{50}) for plated CMs and CMs from CBs. Almost all plated and spontaneously active cells generated APs with a long plateau phase. When the membrane potential was hyperpolarized to −80 mV, durations of evoked APs declined for both types of CMs and a number of previously quiescent cells became active, producing now

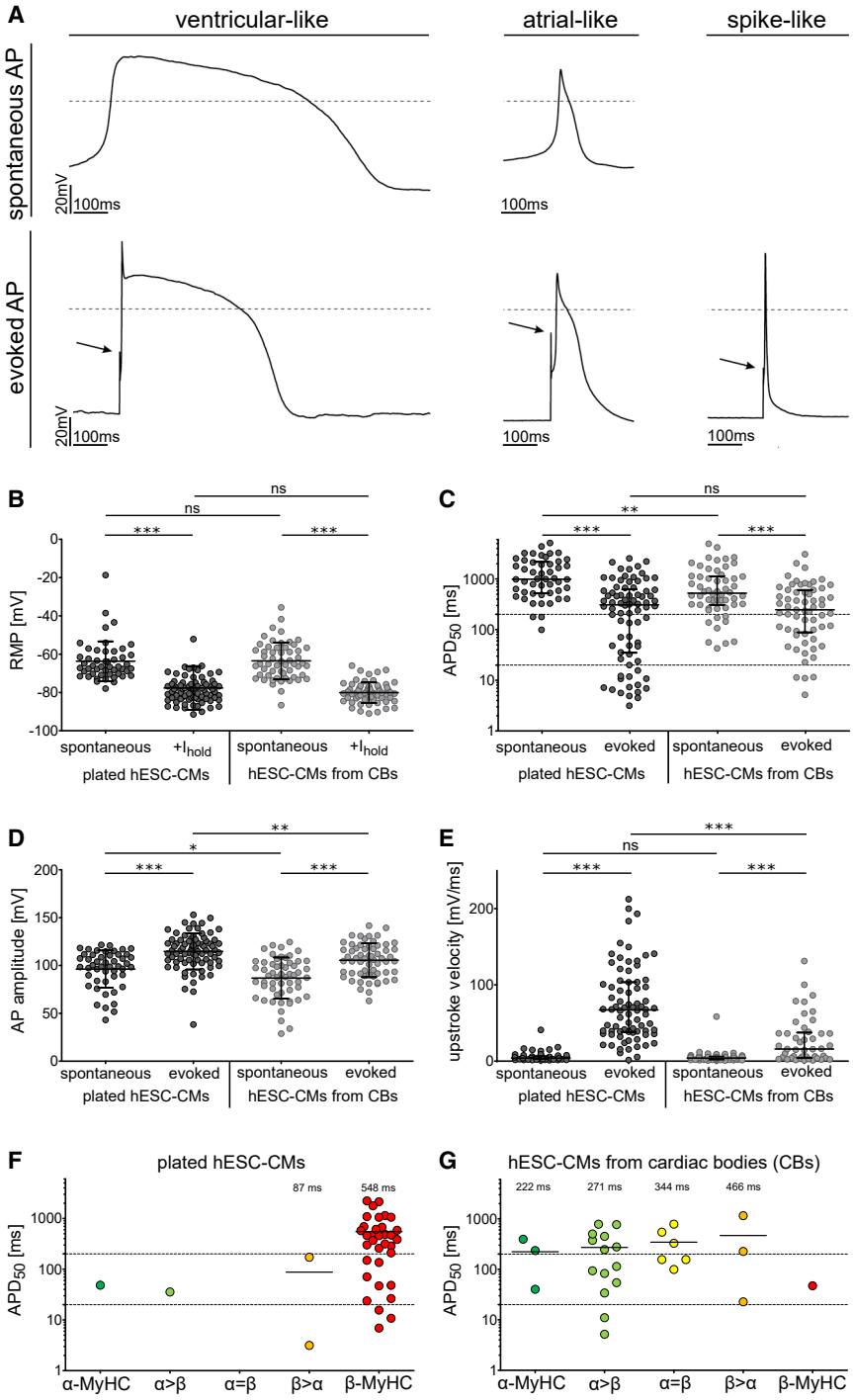

Figure 7. AP Properties Are Independent of α/β-MyHC Isoform Expression in Individual hESC-CMs

(A) Representative patch-clamp recordings of APs from hESC-CMs. Upper traces: spontaneous APs. Lower traces: APs evoked by intracellular stimulation from resting membrane potentials (RMP) around −80 mV. Arrows mark stimulus artifacts. Dashed lines indicate 0 mV. All traces recorded at room temperature.

(B–E) RMP from CMs (B) spontaneously generating APs (n = 49 for plated CMs; n = 56 for CMs from CBs) and from CMs with evoked APs at physiological resting conditions (with RMP about −80 mV, $+I_{hold}$) as adapted by negative holding currents (n = 78 for plated CMs; n = 61 for CMs from CBs). APD_{50} (C), AP amplitudes (D), and AP upstroke velocities (E) from CMs spontaneously generating APs and from CMs with evoked APs (same cell numbers as in B; dotted lines in C indicate APD_{50} values of 20 ms and 200 ms).

(F and G) APD_{50} of the individual retrieved CMs in the different categories of pure α-MyHC- and pure β-MyHC-positive CMs, with three categories of CMs with mixed α/β-MyHC expression (α > β, α = β, α < β). (F) Plated CMs with evoked APs (n = 38) and (G) CMs from CBs with evoked APs (n = 27).

Scatterplots in (C) and (E) include median values ± IQR; in (B), (D), (F), and (G), horizontal lines and numbers above columns indicate mean values ± SD. Statistical significance was tested by Student's t test (B and D) or Mann-Whitney U test (C and E), with *p < 0.05, **p < 0.01, and ***p < 0.001.

See also Figures S3 and S7.

atrial-like, spike-like, or ventricular-like APs. Notably, AP durations strongly depend on temperature, as recently shown for hiPSC-derived CMs (Halloin et al., 2019). Accordingly, AP durations as long as 1,000 ms are typically observed at room temperature only. Raising the temperature to 37°C decreased APD_{50} values to 67–512 ms, while RMP, AP amplitude, and upstroke velocities remained unaffected (Figure S7).

Applying negative holding currents increased the AP amplitudes (Figure 7D) and upstroke velocities (Figure 7E), since sodium channels leave their inactivated state upon repolarization to −80 mV. This experimental procedure is

thus particularly suitable for estimating sodium channel expression in cultivated hESC-CMs. Accordingly, significantly larger upstroke velocities of evoked APs found for plated CMs as compared with CB-derived cells suggest enhanced electrophysiological maturation by prolonged cultivation on a stiff matrix (Weber et al., 2016). Upstroke velocities of spontaneous APs at low resting potentials do not reveal this difference. To test whether MyHC protein isoform expression allows one to predict ventricular-like versus atrial-like APs of hESC-CMs, we extracted from Figure 7C the data of retrieved CMs after immunostaining and plotted AP durations versus α/β-MyHC protein composition of the very same cells (Figures 7F and 7G). Only APD_{50} values but not RMP, AP amplitude, or upstroke velocity are suitable to distinguish between atrial-like and ventricular-like APs. Nearly all retrieved plated CMs showed pure β-MyHC expression, but shapes of evoked APs varied from ventricular-like to atrial-like and spike-like appearance with a correspondingly broad range of AP durations (Figure 7F). Also, hESC-CMs from CBs displayed AP durations above and below 200 ms with no clear relation to the MyHC isoform (Figure 7G). Even though statistical comparison is not feasible with the limited number of CMs per category, the data distribution suggests that the expression of MyHC isoforms and AP-related ion channels are independently regulated in hESC-CMs.

DISCUSSION

In this study we investigated at the single-cell level whether contraction kinetics and electrical activity of hESC-CMs are related to the relative expression of α-MyHC versus β-MyHC. To enable multiparametric analyses of the very same single cells, we established a single-cell mapping technique. In adult human myocardium, pure β-MyHC expression and longer AP duration are characteristic for ventricular CMs. Also, contraction kinetics appear distinct for atrial and ventricular CMs (Narolska et al., 2005), suggesting an influence of MyHC isoform on contraction. Surprisingly, cell-by-cell analysis revealed that in the hESC-CMs, α-MyHC versus β-MyHC expression was not related to specific contractile or electrophysiological properties and thus to atrial versus ventricular phenotype. Furthermore, only a weak correlation between *MYH*-mRNA and MyHC protein isoform abundance in the individual CMs was found.

Single-Cell Mapping Technique

Our mapping technique enables unambiguous, accurate, and highly successful retrieval of individual cells after immunostaining and other experimental procedures, even if applied subsequently to patch clamping, which causes some cell loss. Since the technique is based on a computerized algorithm, cell recovery is independent of the physical setup of applied microscopes and of the carrier used for cell culture. In contrast, location techniques using, e.g., gridded carriers, are usually feasible in only few limited formats and sizes. With the single-cell mapping technique, functional studies carried out in physiological setups for measuring contraction or AP characteristics can also be related cell by cell to, e.g., protein and mRNA expression. Subsequent laser capture microdissection of the individual remapped CMs may even enable single-cell RNA sequencing or single-cell western blotting in relation to the functional studies in individual cells.

Discrepancy between α/β-MyHC Protein Isoform and *MYH6*/*MYH7*-mRNA Expression at the Single-Cell Level

The majority of all cells including pure α-MyHC- or pure β-MyHC-expressing CMs showed variable *MYH6* and *MYH7*-mRNA fractions. Therefore, it is difficult to predict the respective protein isoform expression from *MYH*-mRNA analysis and vice versa. The general mismatch between *MYH*-mRNA and protein expression levels in the same cells suggests that synthesis rates and degradation rates of *MYH*-mRNA and protein are different (Schwanhäusser et al., 2011; Sharova et al., 2009). The *MYH6*-mRNA spots in pure β-MyHC-positive CMs or *MYH7*-mRNA spots in pure α-MyHC-positive CMs could also indicate storage of mRNA in P-bodies, where it may be degraded or stored to re-enter the translation process later on (Hubstenberger et al., 2017).

Relation between MyHC Protein Isoform Expression and hESC-CM Contraction Kinetics

Several studies revealed substantial effects of human cardiac MyHC isoforms onto functional parameters, such as sliding velocity (Noguchi, 2003), ATP turnover, rates of force redevelopment, relaxation, and tension cost (Narolska et al., 2005; Weber et al., 2016), as well as onto sarcomere shortening velocities and amplitudes (Herron et al., 2007). Also, model calculations based on data obtained from rat and porcine CMs suggested that 10%–30% α-MyHC already increases the rate of force development and shortens the time course of isometric twitch contraction (Locher et al., 2009; Rice et al., 2008). However, analysis of twitch kinetics in direct relation to MyHC isoform expression in the present study showed that in hESC-CMs twitch parameters are independent of the MyHC isoform. It is surprising that in the present work and previously (Weber et al., 2016), a consistently shorter ttp or V_{max} was not even observed in hESC-CMs with high fractions of α-MyHC.

Notably, analysis of MLC2a and MLC2v in the same hESC-CM populations suggested that β-MyHC and

MLC2v are rarely co-expressed. Yet there is evidence that sarcomeric contraction parameters also depend on the MLCs associated with the MyHCs (Morano, 1999). The divergent expression of MLCs and MyHCs in the hESC-CMs studied here is different from adult human ventricular CMs and could provide another explanation for the missing correlation between twitch parameters and ventricular versus atrial MyHC isoform expression.

It has been shown that contractile parameters of CMs are affected by the resting SL (Edman, 1979). In the present study, the mean resting SL was the same for exclusively α-MyHC- versus β-MyHC-expressing hESC-CMs, and for plated CMs versus CMs from CBs. Although ttp and hrt seemed to depend on SL, there was no evidence for a systematic effect of culture conditions or MyHC isoform expression on these relationships. Thus, differences in resting SL and morphology of hESC-CMs might contribute to the scatter of the measured twitch parameters but do not explain that twitch kinetics of hESC-CMs were independent of MyHC isoform. Most importantly, the relatively slow kinetics of intracellular calcium transients with ttp similar to that of simultaneously recorded twitches may dominate the kinetics of contraction in hESC-CMs (Weber et al., 2016). This is different from model calculations, which took into account a much faster time course of the calcium transient compared with the twitch (Locher et al., 2009; Rice et al., 2008). For hESC-CMs the slow calcium transients may indicate an immature state of the calcium handling system including the absence of T-tubules (Lieu et al., 2009; Weber et al., 2016), and low expression levels of ryanodine receptors, calcium-storing proteins in the sarcoplasmic reticulum, and sarcoplasmic ER calcium ATPase (Dolnikov et al., 2006; Liu et al., 2007).

The prevailing calcium transients in hESC-CMs imply that development of calcium handling could be a major factor driving ventricular β-MyHC expression and contractile function. In mouse CMs, alterations in intracellular calcium levels influence signaling cascades related to the β-MyHC isoform switch (Molkentin et al., 1998), but in human heart it seems independent of alterations in intracellular calcium (Gupta, 2007). In the present study we observed highly heterogeneous diastolic calcium levels and time courses of intracellular calcium transients for individual plated CMs and CMs from CBs, as shown previously, with no evidence for a relation between MyHC isoform and specific parameters of calcium handling (Weber et al., 2016).

We suggest that mechanosensing of a stiff substrate such as glass and adhesion to extracellular matrix proteins via, e.g., β1-integrin receptors might be the major trigger for β-MyHC isoform switch of plated CMs. This can lead to activation of signaling molecules linked to the integrin receptors, such as focal adhesion kinase, which is able to up-regulate *MYH7* gene and to increase β-MyHC protein expression (Pentassuglia and Sawyer, 2013).

Relation between MyHC Protein Isoform Expression and Electrophysiological Function

Correspondingly, we found that electrophysiological properties of hESC-CMs developed independently of the expressed MyHC isoform in individual CMs. Compared with adult ventricular CMs, hPSC-CMs often display an immature phenotype with more depolarized RMPs, a higher probability of spontaneous firing, and reduced AP upstroke velocities. The expression pattern of ion channels changes during development to finally generate quiescent ventricular CMs with resting potentials around −80 mV and APs with fast initial depolarization. In agreement with previous observations, we assume that in our hESC-CMs, $K_{ir}2.1$ channels, which stabilize low membrane potentials, are inadequately expressed even with long culture times (Lieu et al., 2013). However, different cultivation conditions (plated versus CB) clearly affected AP amplitudes and particularly upstroke velocities, when APs were evoked by intracellular stimulation from a resting potential experimentally adjusted to −80 mV. This suggests that CMs plated on a stiff matrix express more voltage-dependent $Na_v1.5$ sodium channels. Thus, plating of hESC-CMs not only supports expression of the ventricular β-MyHC isoform but most likely also promotes maturation of certain ion channels. Comparison of MyHC staining and AP shape for the very same CMs, however, revealed that maturation of ventricular contractile proteins and ventricular expression of ion channels are not directly linked. AP phenotypes varied considerably as indicated by nearly 100-fold variation of APD_{50} values even in the group of plated CMs with pure β-MyHC. Altogether, our electrophysiological results support the hypothesis that expression of contractile proteins and ion channel composition of the plasma membrane are independently regulated during hESC-CM differentiation, which may also affect the time course of twitch contractions.

In conclusion, our multiparametric cell-by-cell analyses provide evidence that in hESC-CMs expression of α-MyHC or β-MyHC is not related to specific electrophysiological or contractile properties and thus to atrial versus ventricular phenotype of the CMs. This suggests that in hESC-CMs regulation of genes associated with electrical activity, contraction, calcium handling, and even MyHCs and MLCs is not closely linked. Instead, external stimuli such as matrix stiffness and other factors may induce specific signaling pathways for the different genes/proteins. For studies of myofilament function in hPSC-CM models (e.g., in the context of genetic cardiomyopathies), expression of sarcomeric protein isoforms (e.g., MyHC, MLC1/2, cardiac troponins I and T) as in adult CMs, is highly desirable to reliably distinguish mutation effects from functional effects of different sarcomeric

protein isoforms. Even if maturation of protein isoforms cannot be achieved equally in each hPSC-CM, single-cell mapping might enable a direct correlation of myofilament function and protein isoform of the same CM to reliably detect, e.g., mutation effects.

EXPERIMENTAL PROCEDURES

Parameters of twitch contractions and intracellular calcium transients were recorded from single hESC-CMs using a MyoCam system (IonOptix, Milton, MA, USA). APs were recorded by a whole-cell patch-clamp technique (Axopatch 200B; Molecular Devices, San Jose, CA, USA). For FISH, specific probe sets for labeling of *MYH6* and *MYH7*-mRNA (Affymetrix, Santa Clara, CA, USA) were used. Immunostaining of α-MyHC and β-MyHC isoforms occurred with highly specific antibodies. Full details are provided in Supplemental Experimental Procedures.

Single-Cell Mapping

In brief, to retrieve the same CMs at different setups and microscopes, we developed a single-cell mapping technique, which allowed us to correct for shifts and rotations of cell positions on coverslips after different experimental procedures. Full details are provided in Supplemental Experimental Procedures and Figure 1.

Statistical Analysis

Details of performed statistical analyses can be found in Supplemental Experimental Procedures and in the figure legends of the respective figures.

SUPPLEMENTAL INFORMATION

Supplemental Information can be found online at https://doi.org/10.1016/j.stemcr.2020.03.015.

AUTHOR CONTRIBUTIONS

N.W. and K.K.: project design, data acquisition and analysis, manuscript writing; T.H.: data acquisition, figure layout; A.R.: data analysis, manuscript writing; M.F., J.d.l.R., and S.T.: data acquisition and analysis; K.S., B.P., N.P., and M.W.: data acquisition; U.K., A.L., S.G., U.Z., and B.C.: single-cell mapping design, data acquisition; J.D.S., G.W., I.I. and A.H.: human sample preparation; J.M., U.M., B.B., R.Z., and T.K.: project design, manuscript writing. All authors approved the final version of the manuscript.

ACKNOWLEDGMENT

We dedicate this paper to the late B.B., co-author of this paper, whose input was essential at the beginning of this study. We continue holding on to his values and the example he set in his scientific work.

This work was supported by grants from Deutsche Forschungsgemeinschaft (DFG: BR849/31-1, KR1187/21–1, MA2331/16-1, ZW64/4-1 and the Cluster of Excellence REBIRTH DFG EXC62/2, EXC62/3; and KFO311 ZW64/7-1). R.Z. received funding from the German Ministry for Education and Science (grants: 13N14086, 01EK1601A, 01EK1602A), the European Union H2020 program (TECHNOBEAT, grant 66724), and StemBANCC (Innovative Medicines Initiative joint undertaking, grant agreement no. 115439-2, resources of which are composed of financial contribution from the European Union [FP7/2007-2013] and EFPIA companies' in kind contribution). The authors have no disclosures.

Received: December 20, 2018
Revised: March 12, 2020
Accepted: March 17, 2020
Published: April 16, 2020

REFERENCES

Bootman, M.D., Higazi, D.R., Coombes, S., and Roderick, H.L. (2006). Calcium signalling during excitation-contraction coupling in mammalian atrial myocytes. J. Cell Sci. *119* (Pt 19), 3915–3925.

Dolnikov, K., Shilkrut, M., Zeevi-Levin, N., Gerecht-Nir, S., Amit, M., Danon, A., Itskovitz-Eldor, J., and Binah, O. (2006). Functional properties of human embryonic stem cell-derived cardiomyocytes: intracellular Ca^{2+} handling and the role of sarcoplasmic reticulum in the contraction. Stem Cells *24*, 236–245.

Edman, K.A. (1979). The velocity of unloaded shortening and its relation to sarcomere length and isometric force in vertebrate muscle fibres. J. Physiol. *291*, 143–159.

Gorza, L., Mercadier, J.J., Schwartz, K., Thornell, L.E., Sartore, S., and Schiaffino, S. (1984). Myosin types in the human heart. An immunofluorescence study of normal and hypertrophied atrial and ventricular myocardium. Circ. Res. *54*, 694–702.

Gupta, M.P. (2007). Factors controlling cardiac myosin-isoform shift during hypertrophy and heart failure. J. Mol. Cell Cardiol. *43*, 388–403.

Halloin, C., Schwanke, K., Lobel, W., Franke, A., Szepes, M., Biswanath, S., Wunderlich, S., Merkert, S., Weber, N., Osten, F., et al. (2019). Continuous WNT control enables advanced hPSC cardiac processing and prognostic surface marker identification in chemically defined suspension culture. Stem Cell Reports https://doi.org/10.1016/j.stemcr.2019.06.004.

Hatem, S.N., Benardeau, A., Rucker-Martin, C., Marty, I., de Chamisso, P., Villaz, M., and Mercadier, J.J. (1997). Different compartments of sarcoplasmic reticulum participate in the excitation-contraction coupling process in human atrial myocytes. Circ. Res. *80*, 345–353.

Herron, T.J., Vandenboom, R., Fomicheva, E., Mundada, L., Edwards, T., and Metzger, J.M. (2007). Calcium-independent negative inotropy by beta-myosin heavy chain gene transfer in cardiac myocytes. Circ. Res. *100*, 1182–1190.

Hubstenberger, A., Courel, M., Benard, M., Souquere, S., Ernoult-Lange, M., Chouaib, R., Yi, Z., Morlot, J.B., Munier, A., Fradet, M., et al. (2017). P-body purification reveals the condensation of repressed mRNA regulons. Mol. Cell *68*, 144–157 e145.

Iorga, B., Schwanke, K., Weber, N., Wendland, M., Greten, S., Piep, B., Dos Remedios, C.G., Martin, U., Zweigerdt, R., Kraft, T., et al. (2018). Differences in contractile function of myofibrils within human embryonic stem cell-derived cardiomyocytes versus Adult

ventricular myofibrils are related to distinct sarcomeric protein isoforms. Front. Physiol. *8*, 1111.

Jung, G., and Bernstein, D. (2014). hiPSC modeling of inherited cardiomyopathies. Curr. Treat. Opt. Cardiovasc. Med. *16*, 320.

Kane, C., and Terracciano, C.M.N. (2017). Concise review: criteria for chamber-specific categorization of human cardiac myocytes derived from pluripotent stem cells. Stem Cells *35*, 1881–1897.

Lieu, D.K., Fu, J.D., Chiamvimonvat, N., Tung, K.C., McNerney, G.P., Huser, T., Keller, G., Kong, C.W., and Li, R.A. (2013). Mechanism-based facilitated maturation of human pluripotent stem cell-derived cardiomyocytes. Circ. Arrhythm Electrophysiol. *6*, 191–201.

Lieu, D.K., Liu, J., Siu, C.W., McNerney, G.P., Tse, H.F., Abu-Khalil, A., Huser, T., and Li, R.A. (2009). Absence of transverse tubules contributes to non-uniform Ca(2+) wavefronts in mouse and human embryonic stem cell-derived cardiomyocytes. Stem Cells Dev. *18*, 1493–1500.

Liu, J., Fu, J.D., Siu, C.W., and Li, R.A. (2007). Functional sarcoplasmic reticulum for calcium handling of human embryonic stem cell-derived cardiomyocytes: insights for driven maturation. Stem Cells *25*, 3038–3044.

Locher, M.R., Razumova, M.V., Stelzer, J.E., Norman, H.S., Patel, J.R., and Moss, R.L. (2009). Determination of rate constants for turnover of myosin isoforms in rat myocardium: implications for in vivo contractile kinetics. Am. J. Physiol. Heart Circ. Physiol. *297*, H247–H256.

Lundy, S.D., Zhu, W.Z., Regnier, M., and Laflamme, M.A. (2013). Structural and functional maturation of cardiomyocytes derived from human pluripotent stem cells. Stem Cells Dev. *22*, 1991–2002.

Miyata, S., Minobe, W., Bristow, M.R., and Leinwand, L.A. (2000). Myosin heavy chain isoform expression in the failing and nonfailing human heart. Circ. Res. *86*, 386–390.

Molkentin, J.D., Lu, J.R., Antos, C.L., Markham, B., Richardson, J., Robbins, J., Grant, S.R., and Olson, E.N. (1998). A calcineurin-dependent transcriptional pathway for cardiac hypertrophy. Cell *93*, 215–228.

Morano, I. (1999). Tuning the human heart molecular motors by myosin light chains. J. Mol. Med. *77*, 544–555.

Narolska, N.A., van Loon, R.B., Boontje, N.M., Zaremba, R., Penas, S.E., Russell, J., Spiegelenberg, S.R., Huybregts, M.A., Visser, F.C., de Jong, J.W., et al. (2005). Myocardial contraction is 5-fold more economical in ventricular than in atrial human tissue. Cardiovasc. Res. *65*, 221–229.

Noguchi, T. (2003). Myosin from failing and non-failing human ventricles exhibit similar contractile properties. J. Mol. Cell Cardiol. *35*, 91–97.

Pentassuglia, L., and Sawyer, D.B. (2013). ErbB/integrin signaling interactions in regulation of myocardial cell-cell and cell-matrix interactions. Biochim. Biophys. Acta *1833*, 909–916.

Pioner, J.M., Racca, A.W., Klaiman, J.M., Yang, K.C., Guan, X., Pabon, L., Muskheli, V., Zaunbrecher, R., Macadangdang, J., Jeong, M.Y., et al. (2016). Isolation and mechanical measurements of myofibrils from human induced pluripotent stem cell-derived cardiomyocytes. Stem Cell Reports *6*, 885–896.

Racca, A.W., Klaiman, J.M., Pioner, J.M., Cheng, Y., Beck, A.E., Moussavi-Harami, F., Bamshad, M.J., and Regnier, M. (2016). Contractile properties of developing human fetal cardiac muscle. J. Physiol. *594*, 437–452.

Reiser, P.J., Portman, M.A., Ning, X.H., and Schomisch Moravec, C. (2001). Human cardiac myosin heavy chain isoforms in fetal and failing adult atria and ventricles. Am. J. Physiol. Heart Circ. Physiol. *280*, H1814–H1820.

Rice, J.J., Wang, F., Bers, D.M., and de Tombe, P.P. (2008). Approximate model of cooperative activation and crossbridge cycling in cardiac muscle using ordinary differential equations. Biophys. J. *95*, 2368–2390.

Schram, G., Pourrier, M., Melnyk, P., and Nattel, S. (2002). Differential distribution of cardiac ion channel expression as a basis for regional specialization in electrical function. Circ. Res. *90*, 939–950.

Schwanhäusser, B., Busse, D., Li, N., Dittmar, G., Schuchhardt, J., Wolf, J., Chen, W., and Selbach, M. (2011). Global quantification of mammalian gene expression control. Nature *473*, 337–342.

Sharova, L.V., Sharov, A.A., Nedorezov, T., Piao, Y., Shaik, N., and Ko, M.S. (2009). Database for mRNA half-life of 19 977 genes obtained by DNA microarray analysis of pluripotent and differentiating mouse embryonic stem cells. DNA Res. *16*, 45–58.

van Meer, B.J., Tertoolen, L.G., and Mummery, C.L. (2016). Concise review: measuring physiological responses of human pluripotent stem cell derived cardiomyocytes to drugs and disease. Stem Cells *34*, 2008–2015.

Veerman, C.C., Kosmidis, G., Mummery, C.L., Casini, S., Verkerk, A.O., and Bellin, M. (2015). Immaturity of human stem-cell-derived cardiomyocytes in culture: fatal flaw or soluble problem? Stem Cells Dev. *24*, 1035–1052.

Vogel, C., and Marcotte, E.M. (2012). Insights into the regulation of protein abundance from proteomic and transcriptomic analyses. Nat. Rev. Genet. *13*, 227–232.

Weber, N., Schwanke, K., Greten, S., Wendland, M., Iorga, B., Fischer, M., Geers-Knorr, C., Hegermann, J., Wrede, C., Fiedler, J., et al. (2016). Stiff matrix induces switch to pure beta-cardiac myosin heavy chain expression in human ESC-derived cardiomyocytes. Basic Res. Cardiol. *111*, 68.

Wessels, A., Vermeulen, J.L., Viragh, S., Kalman, F., Lamers, W.H., and Moorman, A.F. (1991). Spatial distribution of "tissue-specific" antigens in the developing human heart and skeletal muscle. II. An immunohistochemical analysis of myosin heavy chain isoform expression patterns in the embryonic heart. Anat. Rec. *229*, 355–368.